AIP | The Journal of Chemical Physics

Effect of quenched size polydispersity on the ordering transitions of hard polyhedral particles

Umang Agarwal and Fernando A. Escobedo

Citation: J. Chem. Phys. **137**, 024905 (2012); doi: 10.1063/1.4734021
View online: http://dx.doi.org/10.1063/1.4734021
View Table of Contents: http://jcp.aip.org/resource/1/JCPSA6/v137/i2
Published by the American Institute of Physics.

Effect of quenched size polydispersity on the ordering transitions of hard polyhedral particles

Umang Agarwal and Fernando A. Escobedo[a)]
School of Chemical and Biomolecular Engineering, Cornell University, Ithaca, New York 14853, USA

(Received 22 April 2012; accepted 18 June 2012; published online 12 July 2012)

Monodisperse polyhedral nanocrystals with O_h (octahedral) symmetry self-assemble into various mesophases and crystal structures at intermediate and high concentrations. In this work, the effect of quenched size polydispersity on phase and jamming behavior has been studied via molecular simulations for three representative O_h polyhedral shapes; namely, cubes, cuboctahedrons, and truncated octahedrons. Polydispersity is set by the standard deviation "δ" of an underlying Gaussian distribution of particle sizes, and is "quenched" in that it is fixed in a given uniphase sample. Quenched polydisperse states are relevant to: (i) equilibrium behavior for small enough δ when phase segregation does not occur, and (ii) actual experimental behavior for arbitrary δ when dense states are reached at a rate faster than the relaxation of slow diffusion-driven fractionation modes. Space-filling polyhedrons (cubes and truncated octahedrons) are found to be more robust with respect to the nucleation of orientational and translational order at high polydispersities compared to the non-space-filling cuboctahedron, with the former shapes exhibiting an onset of jamming behavior at a critical polydispersity δ_t that is about twice larger than that for the latter ($\delta_t \approx 0.08$). Further, the orientational ordering in cubes is found to be highly resilient to polydispersity, leading to the formation of a dense, orientationally aligned, and translationally jammed state. Overall, increasing size polydispersity enhances the range of pressures where the mesophases occur. © *2012 American Institute of Physics*. [http://dx.doi.org/10.1063/1.4734021]

I. INTRODUCTION

Recent advances in nanocrystal synthesis[1,2] have made possible the formation of a wide variety of polyhedral shapes belonging to diverse symmetry groups and having varying degrees of anisotropy. Non-spherical nanoparticles can arrange themselves into extended superlattices[3–5] and can also form mesophases with partial order at intermediate packing densities.[6–8] These assemblies exhibit vastly different optical, electronic, physical, and chemical properties[9] depending on nanocrystal size and shape and their superstructure symmetry. Synthesis of colloidal nanoparticles typically results in size polydispersity,[10] which may affect the assembly of superstructures in non-trivial ways. For instance, size polydispersity in hard sphere systems results in formation of glasses[11,12] or fractionation into several coexisting solids[13] with spatially varying average diameter distributions. In length polydisperse rods, partitioning of components and orientational order takes place between the isotropic and nematic phases:[14] In the nematic phase the longer rods concentrate and align but short rods remain orientationally disordered, while in the isotropic phase the longer rods are dilute but form small bundles. Since polyhedrons have both orientational and translational degrees of freedom, polydispersity-induced jamming or segregation may occur with respect to either or both of these kinds of order. To the best of our knowledge, the effect of polydispersity on the phase behavior of polyhedral nanocrystals and its dependence on particle geometry remains unexplored (polydisperse cubes have been studied but only when constrained to be parallel or on a lattice.[15–17]) The present study aims at obtaining a basic understanding of the changes in phase behavior of different polyhedral shapes brought about by the introduction of increasing amounts of quenched polydispersity in their particle size distribution.

A class of polyhedral nanocrystals with O_h symmetry has become readily synthesizable by controlling the growth step in a modified polyol process for the formation of gold nanocrystals.[18–20] The assemblies of these Au nanocrystals have a wide range of applications such as in biosensing, photovoltaics, surface plasmonics, and photothermal therapy.[21–24] The different polyhedral shapes formed at specific growth stages in the formation of cubic Au/Ag nanocrystal vary from that of an octahedron to a truncated octahedron, cuboctahedron, truncated cube, and cube in increasing order of size (as shown in Fig. 1).[18] The phase behavior of the two space-filling members of this class (cubes and truncated octahedrons) has already been established,[6,7] while the phase behavior of other non-space-filling members agrees closely with the guidelines suggested in Ref. 6 regarding the correlation between mesophase type and the two geometry defining parameters: particle shape asphericity and rotational symmetry. It should be pointed out, however, that the liquid-crystal character of a putative cubatic mesophase for cubes at concentrations near the order-disorder transition has recently been called into question.[25] This is based on the observation of an extent of translational order that would be consistent with crystal order (this issue will be revisited later in light of our results). As marked in Fig. 1, truncated cubes show

a)Electronic mail: fe13@cornell.edu.

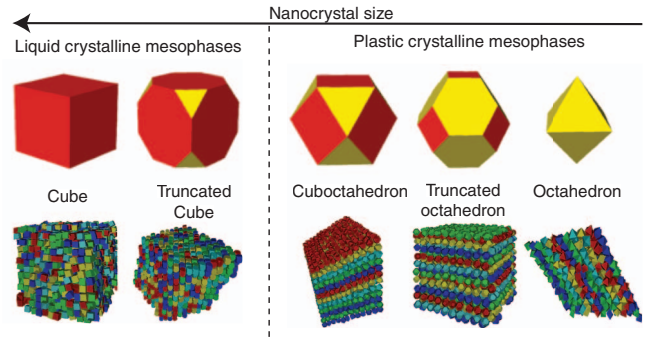

FIG. 1. Nanocrystal shapes synthesized at different growth stages of the modified polyol process. The snapshots show the simulated mesophases at the order-disorder transition point (particle colors are used to highlight layering behavior).

a phase behavior that is very similar to that of the cubes (results shown in Fig. S1 of the supplementary material[26]). Cuboctahedrons and octahedrons show somewhat similar phase behavior as truncated octahedrons[6] with cuboctahderons showing two first-order transitions (instead of one, as in truncated octahedrons[6]) separating the three phases: an isotropic liquid phase, a rotator or plastic crystalline phase (with translational order but no orientational order), and a crystalline solid phase with both kinds of order (Fig. S2 in the supplementary material[26]). Size polydispersity is expected to have a non-trivial effect on the ordered phases of these polyhedra because it will tend to weaken the directional "entropic bonds"[27] responsible for bringing particles together with complementary facets in parallel alignment (thus optimizing packing and maximizing translational entropy) at high concentrations.[6,7]

We chose three shapes: cubes, cuboctahedrons, and truncated octahedrons (which encompass three distinct types of phase behavior) to investigate the effects of quenched polydispersity on the nucleation of orientational and translational order in polyhedral assemblies. The comparison of cubes (that form a liquid crystal mesophase) vs. the other two shapes (that form a plastic crystal mesophase) will address the question: how does size polydispersity affect the establishment of different types of mesophases? The comparison of cuboctahedrons (whose monodisperse densest packing does not tessellate space) vs. truncated octahedrons (whose monodisperse densest packing tessellates space) will address the question: how does size polydispersity affect the establishment of the same types of order (mesophase and crystal) when the original particle shape is either non-space filling or space filling? In this work we are only concerned with "quenched" size polydispersity, wherein the size of any given particle remains fixed throughout (as opposed to being periodically sampled from an underlying distribution), and particles can only locally (pseudo-dynamically) diffuse, and hence no macrophase separation could be detected for the system sizes employed here. As such, our simulations will not capture thermodynamic behavior at conditions where phase partitioning could occur (e.g., for large polydispersities), but will be representative of an experimental scenario where dense states are reached at a rate faster than the relaxation of slow diffusion-driven fractionation modes.

II. METHODS

Particles were assumed to interact via hard-core excluded-volume effects only. Compression runs were used to obtain the phase behavior of each shape for different degrees of polydispersity. Expansion runs for cubes show no hysteresis and the two curves overlap each other as shown Fig. S3 of the supplementary material;[26] for truncated octahedrons and cuboctahedrons a small amount of hysteresis is observed around any first-order order-disorder transition. Isothermal-isobaric *NpT* Monte Carlo (MC) simulations were carried out to obtain the equilibrated structure at each pressure state point. Each shape was simulated for 12 different polydispersity values ($0.02 \leq \delta \leq 0.3$) with the polydispersity parameter δ defined as $\delta = \sqrt{\langle (r_i^2 - 1)^2 \rangle}$, where r_i is the particle-size scaling factor. The desired polydispersity was introduced in the starting random configuration by selecting the size of each particle randomly from a Gaussian distribution with a mean $\langle r_i \rangle = 1.0$, standard deviation δ, and truncated tails (see examples in Fig. S4 of the supplementary material[26]). For each polydispersity, reported results are based on simulations for five independent initial configurations generated this way (agreement between independent runs for cubes is shown in Fig. S5 of the supplementary material[26]). The compression runs were carried out in small increments of osmotic pressure value P^* with increased sampling (smaller pressure steps) near the transition points. The dimensionless osmotic pressure P^* was defined as $P^* = Pa^3/\varepsilon$, where "a" is the radius of the circumscribing sphere (specific to each particle geometry) for a unit scaling ratio $r_i = 1$ and "ε" is an arbitrary energy parameter (set to 1). Relaxation at each pressure is accomplished via translation, rotation, and anisotropic volume moves (which for ordered phases involve changes of the simulation box volume and triclinic shape). Additional "flip" moves[28] that attempt to rotate a chosen particle to a random orientation in a plane perpendicular to its current orientation were also used to increase configurational sampling efficiency. Each Monte Carlo cycle consists of N translation, N rotation, N/10 flip, and 1 volume moves, where N is the total number of particles (which ranged from 1728 to 4096). All moves were accepted or rejected according to the Metropolis criterion, which in this case involves overlap checks using the separating axes theorem.[29] Each pressure run consisted of 3×10^6 Monte Carlo cycles for both equilibration and production. The equilibration at each pressure value was monitored by recording the volume fraction ϕ of the system against simulation cycles, and by checking the convergence of various orientational and translational order parameters measured for configurations periodically saved during the production runs. The phase characterization and analysis of different phases were subsequently done using various translational and orientational order parameters, mobility coefficients, and visual inspection of local order in color-coded snapshots.

The orientational order for cubes was measured using the cubatic order parameter $\langle P_4 \rangle$ defined as:

$$\langle P_4 \rangle = \max_{\hat{n}} \frac{3}{14N} \sum_i P_4 (\hat{u}_i \cdot \hat{n}) = \max_{\hat{n}} \frac{3}{14N} \sum_i (35 \cos^4 \theta_i(\hat{n}) - 30 \cos^2(\hat{n}) + 3), \quad (1)$$

where $\hat{u}_i$ is the unit vector along a relevant particle axis and $\hat{n}$ is a director unit vector which maximizes $\langle P_4 \rangle$. To find $\hat{n}$ and the value of maximum order parameter, we used an approximate numerical recipe detailed in Ref. 7. This recipe yields the director vectors $\hat{n}_1$ and $\hat{n}_2$ which maximize the corresponding values of order parameters $[\langle P_4 \rangle]_1$ and $[\langle P_4 \rangle]_2$ while being maximally orthogonal to each other. The orientational order for truncated octahedrons and cuboctahedrons was estimated via orientational distribution functions as described in the supplementary material of Ref. 6.

To quantify changes in translational order we used various spherical-harmonics-based bond order parameters. The long-range order was measured using the global parameters Q_4 and Q_6 proposed by Steinhardt *et al.*,[30] while to identify local clusters and capture the fractionation of assemblies in different coexisting solid and jammed phases, local parameters[31] $\bar{q}_4(i)$ and $\bar{q}_6(i)$ were used. Both definitions use a rotationally invariant summation over the spherical harmonics of bond vectors formed by the first neighboring shell of particles. The definitions are given by equation sets 2 and 3, respectively,

$$Q_l = \left[\frac{4\pi}{2l+1} \sum_{m=-l}^{l} \left| \bar{Q}_{lm}(\vec{r}) \right|^2 \right]^{\frac{1}{2}}$$

with

$$\bar{Q}_{lm} = \frac{1}{\sum_i N_b(i)} \sum_i \sum_{N_b(i)} Y_{lm}(\vec{r}) \quad (2)$$

and

$$\bar{q}_l(i) = \left[\frac{4\pi}{2l+1} \sum_{m=-l}^{l} |\bar{q}_{lm}(i)|^2 \right]^{\frac{1}{2}}$$

with

$$\bar{q}_{lm} = \frac{1}{N_b(i)} \sum_{k=0}^{N_b(i)} q_{lm}(k)$$

$$q_{lm}(k) = \frac{1}{N_b(k)} \sum_{N_b(k)} Y_{lm}(\vec{r}), \quad (3)$$

where $N_b(i)$ is the number of neighbors of particle i, identified as particles which are at a distance of less than 1.2 times the first peak distance in the radial distribution function g(r), and Y_{lm} are spherical harmonics for the neighboring particles position vector $\vec{r}$ (the angles θ and ϕ for each position vector are defined with respect to an arbitrary laboratory frame). The values of all these parameters are minimal (near zero) for disordered structures and increase depending on the underlying crystal lattice symmetry: Q_4 and $\bar{q}_4(i)$ are maximal for a simple cubic-like lattice while Q_6 and $\bar{q}_6(i)$ are maximal for a FCC or HCP like lattice (with hexagonal layering).

To explore differences in dynamic properties of the assemblies at various pressure values and to capture the jamming behavior of the particles we used a mobility coefficient D, which serves as an effective diffusion constant suitable for Monte Carlo simulations. The coefficient is calculated by determining the rate of change of the mean squared displacements of particles measured in independent constant-density simulations of the equilibrated phase. The simulations are carried out with a fixed set of translation and rotation "pseudo-dynamic" moves for which small perturbative translation and rotation step sizes are predefined (to maintain constant acceptance probabilities) based from the previous NpT simulations. This helps maintaining equivalent frequency of translational and rotational changes at various state points, such that the average extent of motion can be compared over "time" periods in units of MC cycles. The mean square displacement R_s over a pseudo-time of N_s MC cycles is given by

$$R_s = \frac{\sum_{i=1}^{N} \sum_{j=0}^{N_{MC}-N_s} \left| \Delta r^i_{(j+s),j} \right|^2}{N(N_{MC} - N_s)}, \quad (4)$$

where $\Delta r^i_{(j+s),j}$ is the displacement of the centre of mass of ith particle between the jth and $(j+s)$th MC cycle and N_{MC} is the total number of cycles in the MC simulation. Accordingly, the units of the mobility coefficient D are (average) particle diameter square per MC cycle.

To better characterize the translational order in systems with cubic order, we developed a new order parameter, which is similar in spirit to the Lindemann parameter.[32] This new parameter measures average deviation of particle positions from the best-fit set of lattice points defined with respect to individual particle positions, director vectors $\hat{n}_1$ and $\hat{n}_2$ (calculated from maximizing the cubatic order parameter $\langle P_4 \rangle$),[7] and the optimal lattice spacing d (obtained from the first peak of the radial distribution function g(r)). The parameter is defined as

$$\Delta^2_{\text{global}} = \min_i \frac{1}{N} \sum_{j=1}^{N} \min_k \left(\vec{r}_j - \vec{r}^{\,ref}_{i,k} \right)^2,$$

$$r^{ref}_{i,k} = r_i \pm d\{k_1 \hat{n}_1 + k_2 \hat{n}_2 + k_3 \hat{n}_3\}, \quad (5)$$

where $\hat{n}_3 = \hat{n}_1 \times \hat{n}_2$ and k_1, k_2, and k_3 are integers. The $\vec{r}_j$'s are position vectors of the instantaneous particle positions in a given configuration while $\vec{r}^{\,ref}_{i,k}$ is the kth lattice point defined with respect to the ith particle along the three possible director vectors. The first minimization is to find the nearest lattice point for particle j among the various possible reference lattice points $\vec{r}^{\,ref}_{i,k}$'s. The second minimization is to find the particle i which gives most appropriate lattice vectors defined along the orientation of particle i. Note that smaller Δ^2_{global} values correspond to the most ordered states and that one could rescale it to reverse this behavior or to make it be bound between 0 and 1. Another global positional order parameter often employed[25] was also measured by averaging values over

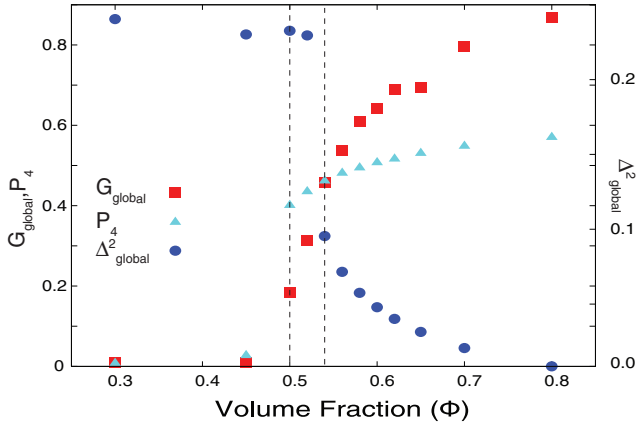

FIG. 2. Different translational and orientational order parameters for assemblies of 8000 cubes at various volume fractions (obtained by sampling over 200 independent configurations from constant density simulations). Dashed lines enclose region of putative cubatic phase character.

all the particles and several configurations,

$$\langle G_{\text{global}} \rangle = \left| \frac{1}{N} \sum_i \exp(i K \cdot \vec{r}_i) \right|, \tag{6}$$

where K is a reciprocal lattice vector of the crystal under consideration (calculated by using the $\hat{n}_1$ and $\hat{n}_2$ director vectors). It can be argued that while Eq. (6) and other similar global order parameters capture the regularity of the "average" particle positions, the order parameter (5) gives instead a sense for the "variance" of the particle positions around their mean values.

III. RESULTS AND DISCUSSION

Perfect monodisperse cubes were reported to have a liquid crystalline "cubatic" mesophase at conditions near the order-disorder transition ($0.51 \leq \phi < 0.54$), characterized by high orientational order, layering along the three directors (indicative of at least intermediate-range translational order), and finite long time translational mobility.[6] A recent study for the same system concludes that the positional ordering near the bulk coexistence regime is long-ranged and indicative of a simple cubic crystal phase but with an unusually high amount of "delocalized" vacancy content (~6.4% (Ref. 25) which is about three orders of magnitude larger than that for typical crystals near the melting transition). While we had also previously quantified and detected significant translational order in such a phase,[6] the finite system sizes did not allow us to ascertain its long-range character and hence the "cubatic" phase designation was adopted based on the dynamic criterion that considers its liquid-crystal-like particle mobility. We have now tried to reassess the positional order in such an unusual phase by performing *NVT* simulations for 8000 cubes at 10 different volume fraction values between $\phi = 0.3$ and $\phi = 0.8$. For the ordered systems, care was taken to ensure that the particle orientation directors had minimal rotation with respect to the cubic box axes. The equilibrated configurations were used to calculate orientational order using $\langle P_4 \rangle$ and translational order using Δ^2_{global} and $\langle G_{\text{global}} \rangle$ as described in Sec. II. For a system of 8000 cubes the ordered phase was

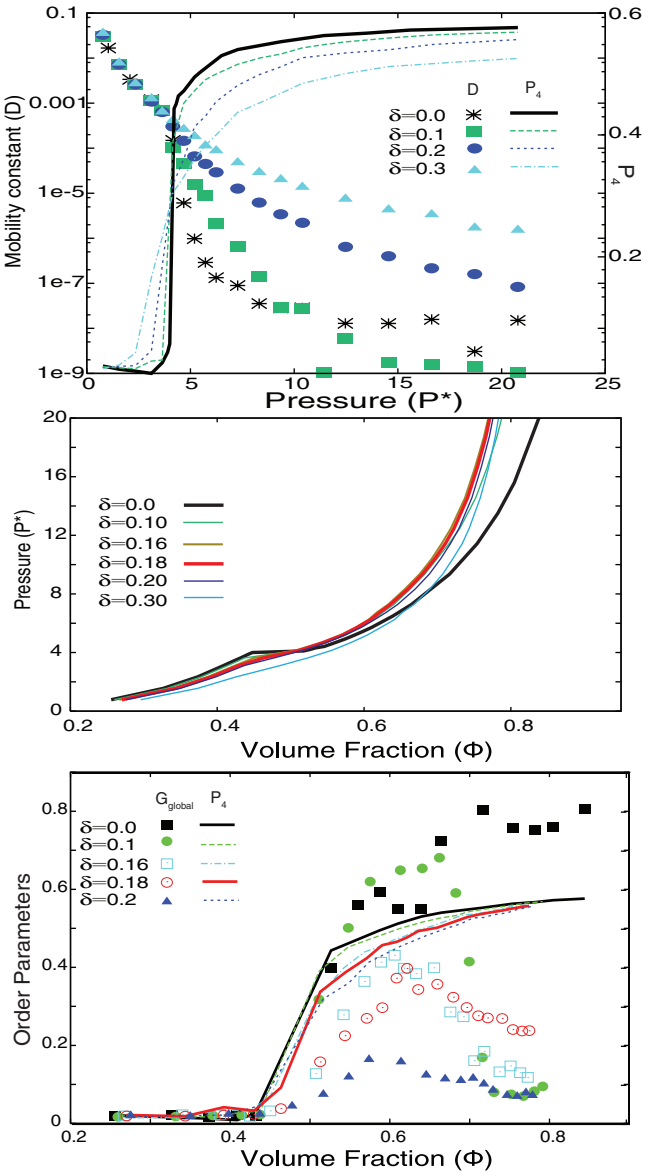

FIG. 3. Polydisperse cubes for $0 \leq \delta \leq 0.3$. (Top) Mobility coefficients (D) and cubatic orientational order parameter $\langle P_4 \rangle$ vs. pressure. (Middle) Equation of state curves showing overlap and no first-order transition density gap for $\delta \geq 0.18$. (Bottom) Translational ($\langle G_{\text{global}} \rangle$) and orientational ($\langle P_4 \rangle$) order parameters vs. volume fraction ϕ; the peak in $\langle G_{\text{global}} \rangle$ around $\phi = 0.6$ indicates conditions that favor structures with cubic symmetry.

estimated[25] to form first at $\phi = 0.5$ (a value slightly overestimated in Ref. 6 due to the smaller sizes used there and the expected finite-size effect). The results reported in Fig. 2 indicate that while the orientational order $\langle P_4 \rangle$ does nucleate at $\phi = 0.5$, the translational order shows a transition to solid-like values at a slightly higher densities around $\phi = 0.54$. In particular, the Δ^2_{global} value for $\phi = 0.52$ is similar to that of an isotropic phase ($\Delta^2_{\text{global}} = 0.23$) and over two times larger than that for $\phi = 0.54$. This happens because Δ^2_{global} is a sensitive probe that detects any transient shifts of the particle positions from their ideal lattice positions. Moreover, efforts to calculate the Lindemann parameter[32] at most of the state points (for $\phi < 0.6$) lead to large and inconsistent values as there is finite diffusion of particles indicative of liquid-like or

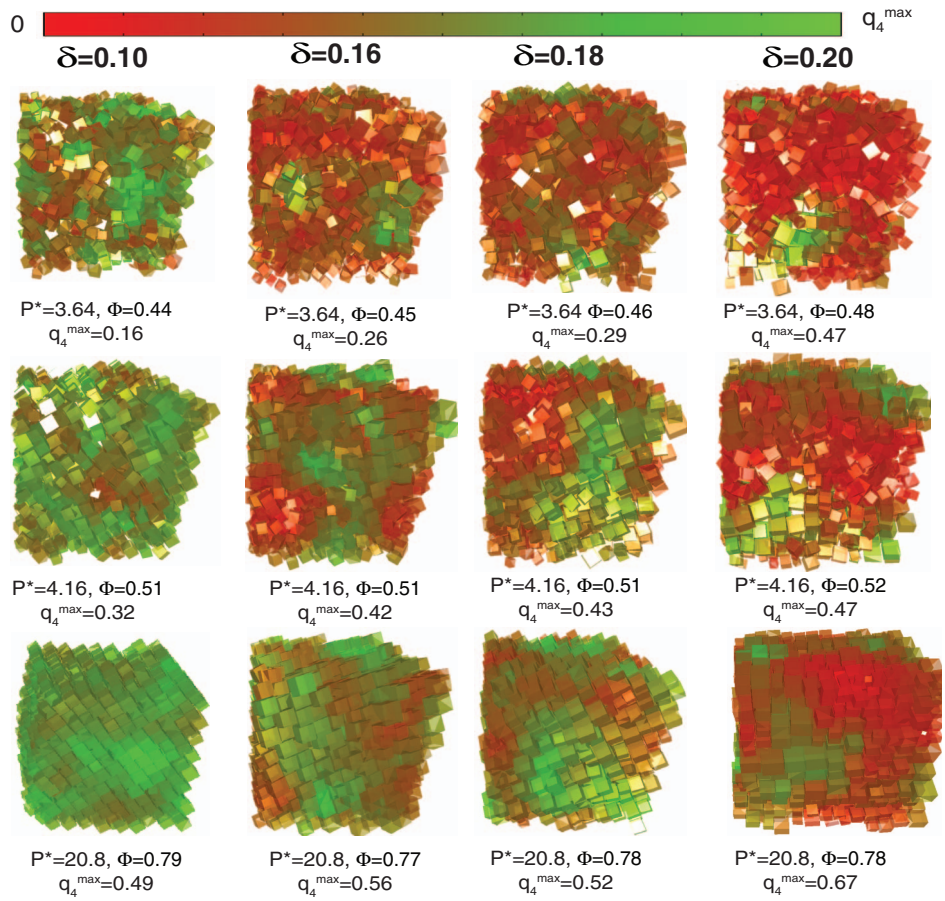

FIG. 4. Snapshots for cubes at various pressures (around the order-disorder transition points, which is significantly different for higher δ systems and higher pressures) for $\delta = 0.10, 0.16, 0.18$, and 0.20. The particles are color coded from red to green, depending on their local bond orientational order parameter value $\bar{q}_4(i)$.

melting behavior with respect to translational order. These results suggest that, at least for $\phi = 0.5$ and 0.52, the phase formed is sufficiently distinct from a cubic crystal and its classification will be contingent to the criteria or threshold order parameter value adopted: while the particles adopt positions which are in *average* somewhat consistent with a cubic crystal (as given by the intermediate $\langle G_{\text{global}} \rangle$ values), the *variance* of their position fluctuations (as given by Δ^2_{global}) is liquid-like.

The effect of polydispersity in the system of cubes is investigated by performing compression runs for 1728 and 4096 cubic particles with quenched size polydispersities varying from $\delta = 0.02$ to 0.30, where δ is the standard deviation of the Gaussian distribution of particle sizes (larger systems were used for larger δ to accommodate a representative sample of particle sizes). The single-phase equation of state (EOS) curves obtained by the compression runs are plotted for the monodisperse system ($\delta = 0$) and for systems with 5 distinct δ values in the middle frame of Fig. 3. (These are "apparent" EOS curves as they would refer to metastable single-phase states in cases when the parent phase can fractionate.) The curves show a density gap associated with the first-order transition until a critical polydispersity value of $\delta_t = 0.18$, after which the transition becomes continuous, suggestive of a translationally jammed state (as observed in spheres[12]). Moreover, the high-density branches of the EOS curves tend to shift left with increasing δ (signaling less efficient pack-

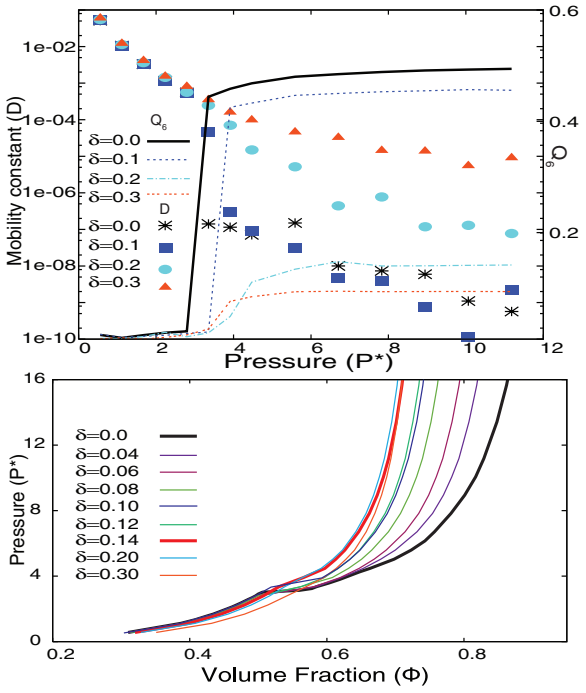

FIG. 5. Polydisperse truncated octahedrons with $0 \leq \delta \leq 0.3$. (Top) Mobility coefficients (D) and global bond orientational order parameter Q_6 plotted against pressure. (Bottom) Equation of state curves showing overlap and no first-order transition density gap for $\delta \geq 0.14$.

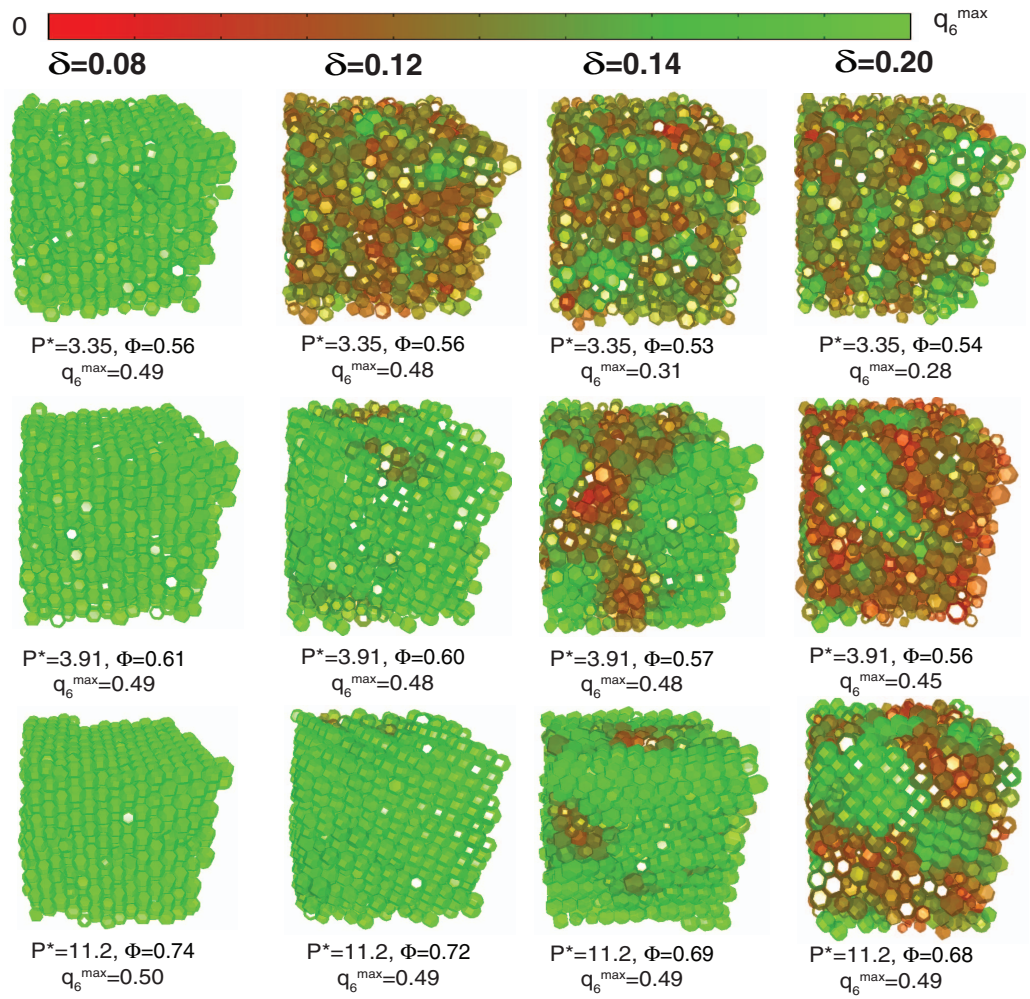

FIG. 6. Snapshots for truncated octahedrons at various pressures (around the order-disorder transition and higher pressures) for $\delta = 0.08$, 0.12, 0.14, and 0.20. The particles are color coded from red to green, depending on their local bond orientational order parameter value $\bar{q}_6(i)$.

ing for a given pressure), and for $\delta \geq 0.18$ show significant overlap with each other, converging toward a packing fraction of $\phi \sim 0.83$ (at $P^* = 103.9$) for most systems. Surprisingly, the low-density "isotropic" branches shift slightly to the right with δ, suggesting a more efficient packing for a given pressure. The mobility coefficient D and the orientational order parameter $\langle P_4 \rangle$ are plotted against the reduced pressure P^* in the top frame of Fig. 3 for $\delta = 0$, 0.10, 0.20, and 0.30. For $\delta = 0.0$ and $\delta = 0.10$, the decay behavior of D shows a transition at $P^* = 4.2$, with the higher density branch decaying to very low D values with pressure. For $\delta = 0.20$ and 0.30, the decay behavior is smoother and the curves plateau (at high pressures) at a value two to three orders of magnitudes higher than that for $\delta = 0.10$, consistent with the notion that diffusion should be larger in systems with less positional order. However, the orientational order parameter $\langle P_4 \rangle$ shows almost perfect alignment for all δ values when $P^* > 4.2$ (top and bottom frames of Fig. 3). Further, the $\langle G_{global} \rangle$ values (bottom frame of Fig. 3) show a non-monotonic dependence with volume fraction ϕ for different polydispersities. While for the monodisperse and low-δ systems the $\langle G_{global} \rangle$ parameter increases mostly monotonically with ϕ, for $\delta \sim 0.10$–0.2 it shows a distinct "broad" peak around $\phi \approx 0.6$–0.63. This peak is indicative of the fact that there is an optimal window of ϕ where the system is sufficiently packed for particles to orientationally align but has still enough free volume to best accommodate polydisperse cubes on a cubic lattice. Once ϕ goes above this window, then the entropic penalty to sustain a cubic translational order becomes too large for a high-δ system, as it approaches a densest packing state where particles must cram into off-lattice positions. It can also be observed that the peak narrows and drops to lower $\langle G_{global} \rangle$ values with increasing δ, disappearing for $\delta > \delta_t$ ($\sim$0.18). These high-δ assemblies result in a novel orientationally ordered high density ($\phi \sim 0.83$) jammed (glass-like) phase.

The local translational order in polydisperse cubes at different state points is analyzed via color-coded snapshots, where each particle is ascribed a color from red to green based on the range of its local bond orientational parameter values $\bar{q}_4(i)$ in going from 0 to q_4^{max} (see Sec. II). The snapshots shown in Fig. 4 for $\delta = 0.18$ and 0.20 show signs of spatial fractionation of particles into solid-like and liquid-like domains (with inhomogeneous size distribution of particles). The jamming behavior at higher densities is noticeable for δ

$= 0.20$ in the form of a high amount of heterogeneities in the local bond order spatial distribution. The growing extent of heterogeneity in such high-δ systems correlates with the increasing trend observed in the D plateau values with δ (shown in Fig. 3), where the liquid-like domains likely become the dominant contributors to the higher mobilities.

Monodisperse truncated octahedrons form a plastic crystalline mesophase for $0.52 < \phi < 0.70$. The nucleation of translational order for this shape precedes that of orientational ordering; hence the effect of introducing polydispersity in these systems is expected to be similar to that for spheres. The apparent EOS curves obtained from compression runs for the monodisperse system ($\delta = 0$) and systems with 8 different δ values are plotted in the bottom frame of Fig. 5. The leftward shift of the solid branches with increasing δ, as in the case of polydisperse cubes, signals the gradual loss of the space-filling ability of the particles. The first-order density gap (separating the isotropic and rotator phases) narrows, disappearing at a critical polydispersity value of $\delta_t \approx 0.14$, above which the curves overlap with each other converging toward a packing fraction of $\phi = 0.73$ (at $P^* = 22.4$). The curves for D and the global bond orientational order parameter Q_6 for $\delta = 0$, 0.10, 0.20, and 0.30, are plotted against the reduced pressure P^* in the top frame of Fig. 5. For $\delta = 0$ and 0.10, the D curve shows a transition at around $P^* = 3.9$, with mobilities decaying to very low values consistent with a crystalline phase at high pressures. For $\delta = 0.20$ and 0.30, the rapid transition in the mobility values disappears, showing instead a continuous slowing down of the dynamics with increasing pressure, with a jamming plateau at mobility values which are three orders of magnitudes higher than that for $\delta = 0.10$. For $\delta = 0$ and 0.10, the Q_6 parameter that measures the amount of translational order in the system shows a sudden transition at $P^* \approx 3.9$ with values converging to $Q_6 \approx 0.5$ and 0.46, respectively. For $\delta = 0.20$ and 0.30, the Q_6 values transition over a wider range of pressure values (above $P^* = 3.9$) and converge to much lower values (around 0.14 and 0.09, respectively). Both D and Q_6 hence suggest formation of a glass-like state for systems with $\delta > 0.14$, characterized by diminishing bond orientational order and slower dynamics (though much higher than the crystalline solid). Orientational order was estimated by plotting orientational distribution functions[6] as shown for selected δ and pressures in Fig. S6(a) of the supplementary material.[26] These functions show that systems with higher δ have less orientational order whether one compares systems at the same pressure or at the same volume fraction; hence, states having limited orientational order consistent with rotator crystals have a higher upper bound in P^* (and ϕ) as δ increases.

To investigate the local ordering and fractionation tendencies at various state points of these polydisperse systems, snapshots with particles color-coded according to their local bond order parameter $\bar{q}_6(i)$ are shown in Fig. 6. The sequence of structures formed around the coexistence point $P^* = 3.91$ indicates localized fractionation of the system into solid- and liquid-like domains above the critical polydispersity value of $\delta_t = 0.14$, whereas for hard spheres fractionation into multiple solid phases is reported to occur at polydispersity values of $\delta_t \sim 0.07$.[13] Note also that the fraction of highly ordered (orientationally and translationally) coexisting solid domains decreases with δ, with negligible crystalline content for $\delta \sim 0.30$.

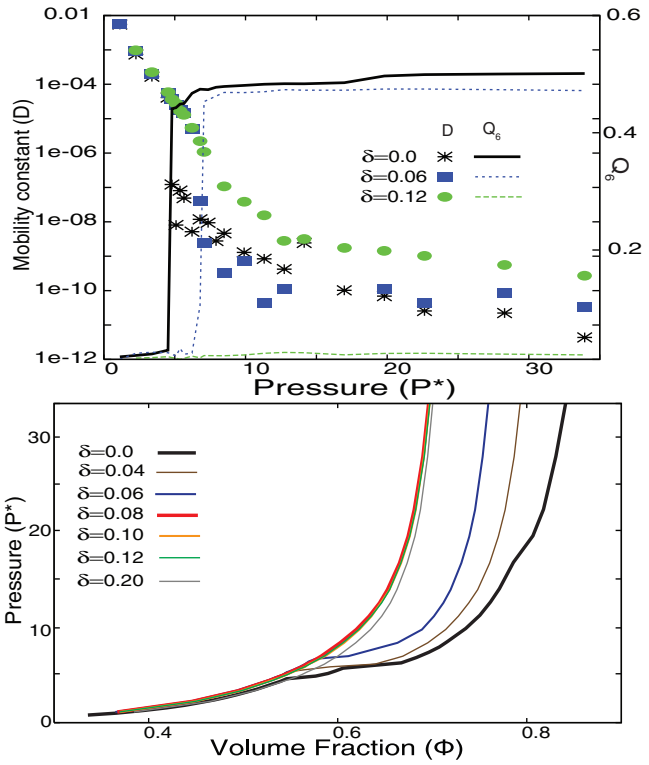

FIG. 7. Polydisperse cuboctahedrons for $0 \le \delta \le 0.20$. (Top) Mobility coefficients (D) and global bond orientational order parameter Q_6 plotted against pressure for $\delta = 0.0$, 0.06, and 0.12. (Bottom) Equation of state curves showing overlap and have no first-order transition density gap for $\delta \ge 0.08$.

Monodisperse cuboctahedrons possess a non-space-filling densest packing having a distorted cubic lattice symmetry, with lattice vectors being permutations of $(-1/3,-1/3,2)$.[4] They exhibit two first-order phase transitions (instead of one as in truncated octahedrons) at around $P^* = 4.0$ and $P^* = 5.4$, separating the branches for the isotropic, rotator, and crystal phases (see Fig. S2 in the supplementary material[26]); the translational order of the rotator phase is harder to characterize unequivocally although it bears resemblance to the distorted cubic lattice of the densest packed state. The apparent single-phase EOS curves obtained from compression runs for the monodisperse case and for systems with 6 different δ values are shown in the bottom frame of Fig. 7. The EOS curves shift to the left with increasing polydispersity, with the rotator-crystal first-order transition disappearing at $\delta = 0.04$ and with the isotropic-rotator transition disappearing for $\delta \ge 0.08$, where all the high-density branches overlap and converge to a packing density of 0.70 (for $P^* = 33.9$). The values of D and the global bond orientational order parameters Q_6 are plotted against pressure P^* for $\delta = 0.0$, 0.06, and 0.12 in the top frame of Fig. 7 (bond orientational plots for $\delta \le 0.06$ are shown in Fig. S7 in the supplementary material[26]). While for $\delta = 0.0$ and 0.06 the D curves exhibit a rapid decay behavior (at around $P^* \sim 6.7$), for $\delta = 0.12$ the decay behavior becomes much more gradual throughout. Moreover, the curve for Q_6 also shows a step-wise increase (rising from ~0.0 to 0.5) at

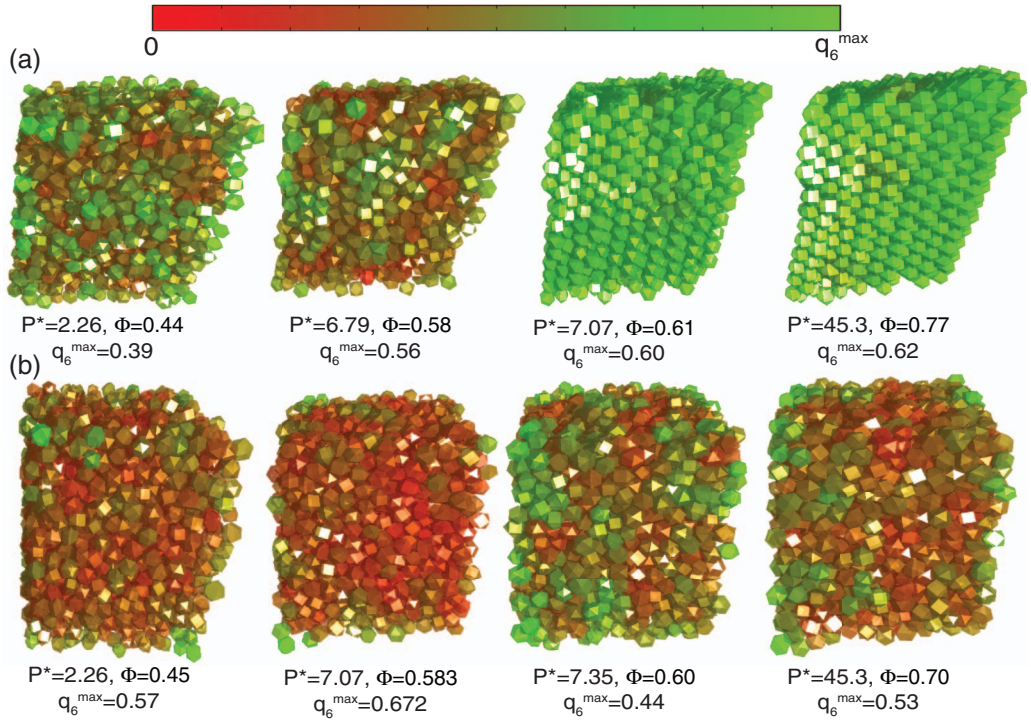

FIG. 8. Snapshots for cuboctahedrons at various pressures (around the order-disorder transition and higher pressures) for (a) $\delta = 0.06$ and (b) $\delta = 0.08$. The particles are color coded from red to green, depending on their local bond orientational order parameter value $\bar{q}_6(i)$.

$P^* \sim 6.7$ for the $\delta = 0.0$ and 0.06 systems, while no increase whatsoever is observed for the $\delta = 0.12$ system. The color-coded snapshots (colors ascribed based on the value of local bond orientational order parameter $\bar{q}_6(i)$) are shown in Fig. 8 at selected pressure state points for the $\delta = 0.06$ and 0.08 systems. While the $\delta = 0.06$ configurations at high-pressure values show a single crystal phase, the $\delta = 0.08$ configurations show particles jamming in a state with no prominent long range or local order. As with truncated octahedrons, the orientational distribution functions for polydisperse cuboctahedrons [see Fig. S6(b) in the supplementary material[26]] show that systems with higher δ have less orientational order for either the same P^* or the same ϕ (with the $\delta = 0.08$ system never attaining any minimal extent of orientational order).

Overall, compared to truncated octahedrons, cuboctahedrons have a behavior more similar to that of hard spheres which also undergo a jamming transition at $\delta_t = 0.08$ into a glassy state with no fractionation into coexisting solid phases.[13] This is unexpected since it is the truncated octahedrons that have an asphericity value (1.291) that is closer to that of spheres (1.0) than cuboctahedrons (1.414). However, a key feature appears to be that cuboctahedrons, like spheres and unlike (monodisperse) truncated octahedrons, do not tessellate space. The stronger entropic bonding associated with a space-filling polyhedron seems to provide added resilience to the structural order and better tolerance of the perturbations in regular packing brought about by size polydispersity. This is further reflected in the fact that for $\delta = 0.08$, for example, cubes and truncated octahedrons can attain denser (more efficient) packing with less jamming than cuboctahedrons at comparable high pressures.

IV. CONCLUSIONS

The introduction of quenched size polydispersity has vastly different effects on the phase behavior (at low δ values) and dynamic arrest behavior (for high δ values) of polyhedrons with different geometries. For cubes, which exhibit an orientational ordering transition before translational ordering upon increasing concentration, the orientational order is preserved even at very high polydispersities. This leads to the formation of a novel orientationally aligned but translationally jammed high-density glassy phase. Truncated octahedrons and cuboctahedrons, which undergo translational ordering before orientational ordering with increasing concentration, form jammed states at lower packing densities and with no long-range orientational or translational order. It can be conjectured that the type of order (orientational or translational) that ensues first upon compression gives an indication of the dominant entropic force driving the ordering of a particular type of polyhedron and hence it will be the most resilient to fight back the disordering effect of increasing size polydispersity. To a first approximation, increasing size polydispersity has an effect that is opposite to that of increasing concentration in the monodisperse system, mainly because increasing δ weakens the packing entropy that drives order, resulting in reduced equilibrium packing fraction of the mesophase or crystal for a given pressure. Quenched polydispersity also enhances the range of conditions (e.g., pressures) where the mesophase in the monodisperse system occurs; i.e., in the limit where δ is at or slightly below δ_t, the entire ordered branch of the equation of state could be said to be a mesophase (a cubatic-like state for cubes and a "rotator" solid

with limited orientational order for the truncated octahedrons and cuboctahedrons).

Cubes and truncated octahedrons, which are space filling when monodisperse, have a significantly larger critical polydispersity δ_t (above which translational order tends to vanish) than the non-space-filling cuboctahedrons. This difference is especially meaningful in comparing truncated octahedrons and cuboctahedrons which exhibit a very similar monodisperse phase behavior. It can be argued that space-filling polyhedrons encode a stronger entropic driving force toward ordering and can hence better counter the "disordering" effect of polydispersity. Furthermore, cubes and truncated octahedrons have a stronger tendency than cuboctahedrons to fractionate into small solid like clusters coexisting with disordered fluid or glassy phase (at higher pressures) for polydispersity values right above δ_t. This difference in behavior can again be ascribed to the stronger driving force to pack efficiently when a cluster of similarly sized particles of nearly space-filling geometry are in proximity. Altogether, these observations support the tenet that space-filling polyhedrons are ideal candidates to form robust self-assembled structures[6] and would be well suited to tolerate particle size imperfections in real systems.

Regarding the ordering behavior of monodisperse cubes, our analysis suggests that a system at conditions around the $\phi = 0.52$ density constitutes a truly unusual state of matter that challenges our conventions for the classification of crystals and liquid crystals. Whether one should call it a "liquid-crystal with an unusually high positional order" or a "crystal with unusually high delocalized-vacancy content and particle mobility" seems a semantic issue that should underscore the unique nature of such a phase.

The present study constitutes a first step toward a road map that elucidates and catalogs all the possible effects that size polydispersity may have on the phase and dynamic arrest behavior of polyhedral assemblies. In this context, it is pointed out again that macrophase fractionation states are practically precluded in these simulations. For small δ values, it is expected that fractionation (from a fixed parent δ) will only occur in a very narrow range of pressures around phase transitions and hence the single-phase behavior simulated here captures thermodynamic behavior. For large δ (certainly above δ_t) single-phase states will likely be metastable over broad ranges of pressures (and densities). The mapping of two-phase states is the object of our ongoing studies, and entails the use of much larger system sizes with special moves to accelerate particle diffusion, and complementary two-box ensemble methods.[11,14] Our purpose for probing such a broad range of quenched polydispersity values in this work was mainly to obtain approximate polydispersity thresholds where structural order and mobility showed marked changes relative to the monodisperse system behavior. Also, the heterogeneous states described here are relevant to real experiments when dense states are reached at a rate faster than the slow diffusion-driven phase segregation. Further studies exploring the effects of different types of polydispersity via semi-grand type of ensembles[11,14] and the effect of enthalpic interactions should provide a more detailed and thorough understanding of the self-assembly process of these highly functional polyhedral nanocrystals.

ACKNOWLEDGMENTS

This work was supported by the U.S. National Science Foundation Grant No. CBET 1033349. The authors gratefully acknowledge helpful discussions with Professor Tobias Hanrath.

[1] Y. Xia, Y. Xiong, B. Lim, and S. E. Skrabalak, Angew. Chem. Int. Ed. **48**, 60 (2009).
[2] Y. G. Sun and Y. N. Xia, Science **298**, 2176–2179 (2002).
[3] S. Sun, C. B. Murray, D. Weller, L. Folks, and A. Moser, Science **287**, 1989 (2000).
[4] S. Torquato and Y. Jiao, Phys. Rev. E **80**, 041104 (2009).
[5] K. F. Bian, J. J. Choi, A. Kaushik, P. Clancy, D. M. Smilgies, and T. Hanrath, ACS Nano **5**, 2815–2823 (2011).
[6] U. Agarwal and F. A. Escobedo, Nat. Mater. **10**, 230–235 (2011).
[7] B. S. John and F. A. Escobedo, J. Chem. Phys. **128**, 044909 (2008).
[8] P. F. Damasceno, M. Engel, and S. C. Glotzer, ACS Nano **6**, 609 (2012).
[9] C. Burda, X. Chen, R. Narayanan, and M. A. El-Sayed, Chem. Rev. **105**, 1025 (2005); C. Salzemann, I. Lisiecki, A. Brioude, J. Urban, and M.-P. Pileni, J. Phys. Chem. B **108**, 13242 (2004).
[10] J. Legrand, A. T. Ngo, C. Petit, and M.-P. Pileni, Adv. Mater. **13**, 58 (2001).
[11] D. A. Kofke and P. G. Bolhuis, Phys. Rev. E **59**, 618 (1999).
[12] T. Nogawa, N. Ito, and H. Watanabe, Phys. Rev. E **82**, 021201 (2010).
[13] M. Fasolo and P. Sollich, "Equilibrium phase behavior of polydisperse hard spheres," Phys. Rev. Lett. **91**, 068301 (2003).
[14] F. A. Escobedo, J. Chem. Phys. **118**, 10262 (2003).
[15] M. Dijkstra, D. Frenkel, and J.-P. Hansen, J. Chem. Phys. **101**, 3179 (1994).
[16] A. Buhot and W. Krauth, Phys. Rev. Lett. **80**, 3787 (1998).
[17] J. A. Cuesta, Phys. Rev. Lett. **89**, 145701 (2002).
[18] D. Seo, J. C. Park, and H. Song, J. Am. Chem Soc. **128**, 14863–14870 (2006).
[19] O. C. Compton and F. E. Osterloh, J. Am. Chem. Soc. **129**, 7793–7798 (2007).
[20] D. Y. Kim, S. H. Im, O. O. Park, and Y. T. Lim, Cryst. Eng. Commun. **12**, 116–121 (2010).
[21] Y. Cao, R. Jin, and C. A. Mirkin, Science **297**, 1536 (2002).
[22] B. D. Moore, L. Stevenson, A. Watt, S. Flitsch, N. J. Turner, C. Cassidy, and D. Graham, Nat. Biotechnol. **22**, 113 (2004).
[23] K. Kneipp, Y. Wang, H. Kneipp, L. T. Perelman, I. Itzkan, R. R. Dasari, and M. S. Feld, Phys. Rev. Lett. **78**, 1667 (1997).
[24] A. J. Haes and R. P. Van Duyne, J. Am. Chem. Soc. **124**, 10596 (2002).
[25] F. Smallenburg, L. Filion, M. Marechal, and M. Dijkstra, e-print arXiv:1111.3466v3.
[26] See supplementary material at http://dx.doi.org/10.1063/1.4734021 for additional plots depicting the changes in pressure and various order parameters with concentration for both monodisperse and polydisperse cubes, cuboctahedra, and truncated octahedra.
[27] See http://www.nsf.gov/awardsearch/showAward.do?AwardNumber=0553719 for a description of the concept of "entropic bond" (abstract posted in 2006).
[28] R. Blaak, D. Frenkel, and B. M. Mulder, J. Chem. Phys. **110**, 110652–11659 (1999).
[29] E. G. Golshtein and N. V. Tretakov, *Modified Lagrangians and Monotone Maps in Optimization* (Wiley, New York, 1996).
[30] P. J. Steinhardt, D. R. Nelson, and M. Rochetti, Phys. Rev. B **28**, 783–805 (1983).
[31] W. Lechner and C. Dellago, J. Chem. Phys. **129**, 114707 (2008).
[32] C. Chakravarty, P. G. Debenedetti, and F. H. Stillinger, J. Chem. Phys. **126**, 204508 (2007).